Optical dephasing of coherent intersubband transitions in a quasi-two-dimensional electron gas

I. Waldmüller, J. Förstner, S.-C. Lee, and A. Knorr
Institut für Theoretische Physik, Nichtlineare Optik und Quantenelektronik, Technische Universität Berlin, 10623 Berlin, Germany

M. Woerner, K. Reimann, R. A. Kaindl,* and T. Elsaesser
Max-Born-Institut für Nichtlineare Optik und Kurzzeitspektroskopie, 12489 Berlin, Germany

R. Hey and K. H. Ploog
Paul-Drude-Institut für Festkörperelektronik, 10117 Berlin, Germany
(Received 22 December 2003; published 13 May 2004)

We present a microscopic many-particle theory for the dephasing of coherent intersubband excitations in semiconductor quantum wells including carrier-carrier and carrier-phonon scattering and light propagation effects. The contributions of many-particle processes are nonadditive and thus cannot be treated separately. It is shown that due to nondiagonal correlation contributions, scattering rates alone cannot be taken as a measure for the dephasing of the intersubband polarization. Surprisingly, radiative damping is found to be important even at moderate carrier densities. Calculated absorption spectra are in excellent agreement with experiments on a high-quality sample.

DOI: 10.1103/PhysRevB.69.205307 PACS number(s): 78.67.De, 73.21.Fg

I. INTRODUCTION

The dynamics of optical excitations of semiconductors on ultrafast time scales gives insight into the basic microscopic interactions of carriers. In particular, optically induced coherence between two electronic bands and its subsequent decay, i.e., optical dephasing, reflects the formation and relaxation of many-particle correlations.[1] In this context, the renormalization of the single-particle properties of Bloch electrons and optical dephasing via electron-electron and electron-phonon interaction has been attributed to the interaction of the optically generated carriers in momentum space. It is a widespread belief that every scattering event a particle undergoes will result in a loss of all phase coherences in which the particle participates. As has been pointed out for interband transitions from the valence to the conduction band [Fig. 1(a)], this simplified picture completely neglects possible interference phenomena between various scattering mechanisms, the nondiagonal correlations between particles in the language of many-particle theory.[2] Such interference phenomena are also significant in quasi-two-dimensional (2D) semiconductor nanostructures where quantum confinement leads to the formation of subbands within the valence and conduction bands. We focus here on dipole-allowed intersubband (IS) transitions[3] between two subbands in the conduction band.

Coherent optical IS polarizations are connected with a quantum mechanical superposition of the envelope wave functions of the subbands involved. When the subbands are parallel [Eq. (7) and Fig. 1(b), solid curves], and in the limit where the Coulomb and Fröhlich matrix elements approach the two-dimensional case [see Eq. (10)], the quantized electron motion perpendicular to the layers is completely decoupled from the free motion in the quantum well plane. In this case, intrasubband electron-electron and electron-phonon interactions do not affect IS coherence. This can be seen by considering a coherent polarization $p_{\mathbf{k}}^{21}$ between subbands 1 and 2 at some in-plane wave vector $\mathbf{k}$. Such a coherent polarization means that the particle is in a superposition state $\alpha|1,\mathbf{k}\rangle+\beta|2,\mathbf{k}\rangle$. Scattering processes that have identical matrix elements for the two subbands [in the approximation of Eq. (10) this is the case for all intrasubband scattering processes] scatter this particle to a new coherent superposition $\alpha|1,\mathbf{k}'\rangle+\beta|2,\mathbf{k}'\rangle$ at another in-plane wave vector $\mathbf{k}'$. This destroys the coherent polarization at $\mathbf{k}$, but at the same time generates a new coherent polarization with identical magnitude and phase at $\mathbf{k}'$. Since the two subbands are parallel, the newly generated coherent polarization is at the same frequency as the destroyed polarization. Therefore the macroscopic polarization, which is obtained by summing over all $\mathbf{k}$, remains unchanged.

In real quantum wells, there are deviations from Eqs. (7) and (10), and thus both intrasubband and intersubband scattering mechanisms have a destructive influence on IS coherence. Intrasubband scattering influences IS coherence only because of these deviations. Its influence is considerably smaller than expected from the scattering rates. The deviations originate (i) from the three-dimensional character of the intersubband and intrasubband scattering matrix elements and (ii) from the difference in the curvature of the subbands [Fig. 1(b), dashed curve], due to the conduction band

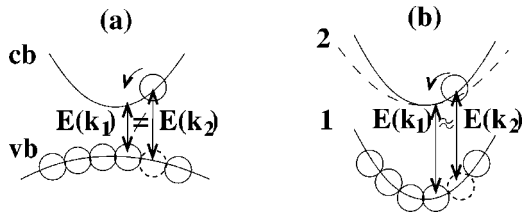

FIG. 1. (a) Interband transitions: transitions between conduction and valence band, (b) IS transitions: transitions between two conduction subbands with equal (solid curve) or with different (dashed curve) effective masses.

nonparabolicity.[4] The latter effect is quite pronounced in InAs/AlSb quantum wells,[5] but as will be shown in the following should not be neglected in GaAs/AlGaAs quantum wells either. In addition to dephasing, radiative coupling of IS polarizations, e.g., in multiple quantum wells (MQW's), leads to emission and exchange of transverse radiation fields, i.e., a mechanism of *radiative damping*.

Recent theoretical work on IS excitations can be divided into different groups: calculations of the IS absorption line shape with regard to a simultaneous treatment of (i) the different curvatures of the subbands and longitudinal Coulomb interaction between electrons,[6–9] (ii) radiative coupling[10,11] using a phenomenological susceptibility, and (iii) dephasing models considering only diagonal dephasing contributions.[12] A comparison of experiment and theory for IS plasmon linewidths below the longitudinal-optical (LO) phonon threshold is given in Ref. 13. To the best of our knowledge, there exists no complete theory which gives a consistent approach to the many-body dephasing by combining the solution of Maxwell's equations (including the transverse radiation field and the longitudinal Coulomb interaction) with a microscopic material theory.

In this paper we present a microscopic theory for the interplay of the basic many-particle interactions. All parts are combined consistently: we compute IS absorption line shapes and linewidths by including the different curvatures of the subbands, Coulomb interaction, radiative coupling, and the major dephasing contributions [electron-electron and electron-phonon (LO) scattering] self-consistently without phenomenological parameters.[14] We examine the validity of the developed theory by a detailed comparison with absorption measurements of a high-quality sample and show that *only a consistent description of all processes can explain the observed line shapes*.

II. EXPERIMENTAL SETUP

Since radiative coupling depends on the actual geometry of the sample, before presenting the theoretical framework we describe first the experimental setup which we use for the absorption measurements. Our sample is a multiple quantum well sample consisting of 51 GaAs quantum wells, each with width $L=10$ nm, and separated by $Al_{0.35}Ga_{0.65}As$ barriers, each with a thickness of $D-L=20$ nm (Fig. 2). The center of each barrier is *n*-type δ-doped with Si, resulting in an electron concentration of $n_e=5\times10^{10}$ cm^{-2} in each quantum well.

The sample was processed into a prism [cf. Fig. 1(c) in Ref. 15] and mounted in the total-reflection geometry (single-pass prism geometry) shown in Fig. 2. This achieves a strong coupling between the *p*-polarized light and the intersubband transition dipoles. Midinfrared absorption spectra were measured using a Biorad FTS 45-A Fourier transform spectrometer. The samples were mounted inside a closed-cycle cryostat equipped with broadband KRS-5 windows to allow measurements at different sample temperatures. A small aperture with razor blade edges ensures that light is only transmitted through the sample facets. Furthermore, a broadband wire-mesh polarizer allows to obtain polarization-dependent spectra both for *p* polarization (the electric field has a component perpendicular to the quantum well layers) and for *s* polarization (electric field parallel to the quantum well layers). This serves to clearly identify intersubband transitions, since they are dipole-allowed only for *p* polarization.

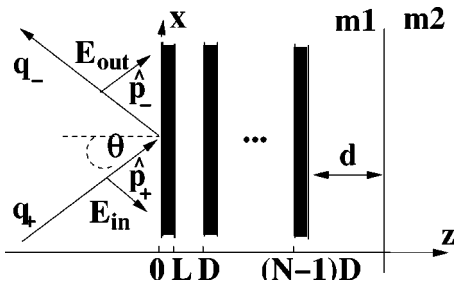

FIG. 2. Single-pass prism geometry: MQW system with respect to total reflection at a medium-1/medium-2 interface in order to enhance the absorption (standing wave): $\mathbf{E}_{in}=E_{in}\hat{\mathbf{p}}_+e^{i\mathbf{q}_+\cdot\mathbf{r}}$ ($\mathbf{E}_{out}=E_{out}\hat{\mathbf{p}}_-e^{i\mathbf{q}_-\cdot\mathbf{r}}$) denotes the ingoing (outgoing) *p*-polarized field (cf. Appendix A). In the experiment the spacing between the last well and the prism base (medium-1/medium-2 interface) is $d=1.26$ μm to center the wells at the antinode of the standing wave, and the angle of incidence is $\theta=63°$.

III. THEORETICAL FRAMEWORK

The absorption spectrum of the sample in the experimental setup described above (see Fig. 2) is given by $A(\omega)=1-|\mathbf{E}_{\rm out}|^2/|\mathbf{E}_{\rm in}|^2$. The calculation of the absorption spectrum is composed of two parts. The first part involves the determination of the source of the electromagnetic emission in each quantum well, i.e., the dipole density $\mathbf{P}^{(n)}$ [the superscript (n) labels the quantum well]. The second part consists of computing the field $\mathbf{E}^{(n)}$ in each quantum well and the outgoing field $\mathbf{E}_{\rm out}$. The equations for the dipole densities and the fields are coupled and must be solved self-consistently.

To determine the fields, a nonlocal Green's-function formalism[10,16] is applied to a system of N electronically uncoupled quantum wells. The local field $\mathbf{E}^{(n)}$ inside quantum well n consists not only of the incident field $\mathbf{E}_{\rm in}$, but also of the field emitted by the dipole densities in all wells.[17] Expressions for these fields and the outgoing field $\mathbf{E}_{\rm out}$ are given in Appendix A. They show explicitly their dependence on the dipole densities $\mathbf{P}^{(n)}$. The interaction of the emitted fields with the dipole densities represents the influence of radiative interaction on the absorption spectrum. The interaction of the dipole density in a given well with the field emitted in the same well is the self-interaction.

To evaluate $\mathbf{P}^{(n)}$, the dipole density driven by the total field $\mathbf{E}^{(n)}(z,\omega)$ in quantum well n, we define

$$\mathbf{P}^{(n)}(z,\omega)=\frac{1}{\mathcal{A}}\sum_{\mathbf{k}}p_{\mathbf{k}}^{(n)21}(\omega)\mathbf{d}_{21}^{(n)}(z) \tag{1a}$$

$$=\int_{(n)}\vec{\chi}_{z,z'}^{(n)}(\omega)\cdot\mathbf{E}^{(n)}(z',\omega)dz' \tag{1b}$$

$$\vec{\chi}^{(n)}_{z,z'}(\omega) := \frac{1}{\mathcal{A}\hbar}\chi^{(n)}(\omega)\mathbf{d}^{(n)}_{21}(z)\mathbf{d}^{(n)}_{21}(z'). \tag{2}$$

Equation (1a) shows that $\mathbf{P}^{(n)}$ is determined by the intersubband coherence $p^{(n)21}_{\mathbf{k}} = \langle a^{\dagger}_{2k} a_{1k}\rangle$ which we evaluate (see Appendix B) within a many-particle density matrix theory,[2,18,19] in the rotating wave approximation. Here $a^{\dagger}_{2\mathbf{k}}$ ($a_{1\mathbf{k}}$) denotes the creation (annihilation) operator of an electron in subband 2 (1). $\mathcal{A}$ is the area. $\int dz\, \mathbf{d}^{(n)}_{21}(z)$ is the dipole matrix element, $\vec{\chi}^{(n)}_{z,z'}(\omega)$ is the nonlocal susceptibility tensor in dyadic form, and $\chi^{(n)}(\omega)$ is the general linear susceptibility in quantum well n (see Appendix C). $\chi^{(n)}(\omega)$ is defined in terms of $p^{(n)21}_{\mathbf{k}}$ and can be evaluated once the intersubband coherences are determined.

To calculate the intersubband coherences we start by deriving the equation of motion (see Appendix B) for $p^{(n)21}_{\mathbf{k}}$. The starting point for this derivation is the Robertson equation[20] and the Hamiltonian of the system. In the Hamiltonian, we include terms for the energies of the noninteracting electrons and LO phonons, the carrier-field interaction, the Coulomb interaction of the electronic system, and the electron–LO-phonon interaction. A detailed description of the Hamiltonian is given in Appendix B. Because of the Coulomb [Eq. (B1c)] and electron-phonon [Eq. (B1d)] interactions, the intersubband coherence is coupled to higher-order operator terms yielding an infinite hierarchy of equations. This hierarchy must be truncated at some stage in order to obtain a closed set of equations.[1,18] For simplicity we give here only a schematic outline of the equation of motion for $p^{(n)21}_{\mathbf{k}}$ and refer the interested reader to Appendix B. [Note that from now on the index (n) in $p^{(n)21}_{\mathbf{k}}$ will be suppressed for conciseness.]

The equation of motion for the intersubband coherence is written as

$$\frac{d}{dt}p^{21}_{\mathbf{k}} = \frac{d}{dt}p^{21}_{\mathbf{k}}|_{0,\mathrm{cf}} + \frac{d}{dt}p^{21}_{\mathbf{k}}|_{\mathrm{MF}} + \frac{d}{dt}p^{21}_{\mathbf{k}}|_{\mathrm{corr}}. \tag{3}$$

In addition to free-carrier and carrier-field contributions (0, cf), we include first- and second-order carrier-carrier and carrier-phonon contributions. While the first-order (mean-field, abbreviated MF in the following) contributions (exchange self-energy, excitonic enhancement, and depolarization effect[7,8,21]) renormalize the free-carrier and carrier-field contributions, the second-order (correlation, abbreviated as corr) contributions yield a dephasing of the macroscopic polarization. These correlation contributions are quite lengthy and are given in Appendix B. They consist of diagonal terms which depend on the intersubband coherence $p^{21}_{\mathbf{k}}$ at momenta $\mathbf{k}$, and nondiagonal terms which depend on the intersubband coherence at different momenta $\mathbf{k}+\mathbf{k}''$, and thus couple different k states of the intersubband coherence:

$$\frac{d}{dt}p^{21}_{\mathbf{k}}|_{\mathrm{corr}} = -\frac{\pi}{\hbar}\Xi_{\mathrm{d}}(p^{21}_{\mathbf{k}}) + \frac{\pi}{\hbar}\sum_{\mathbf{k}''}\Xi_{\mathrm{nd}}(p^{21}_{\mathbf{k}+\mathbf{k}''}). \tag{4}$$

The diagonal terms can be decomposed into in- and outscattering rates:

$$\Xi_{\mathrm{d}}(p^{21}_{\mathbf{k}}) = \Gamma_{\mathrm{d}}p^{21}_{\mathbf{k}} = \frac{1}{2}\sum_{i=1,2}(\Gamma^{i,\mathrm{out}}_{\mathrm{d}} + \Gamma^{i,\mathrm{in}}_{\mathrm{d}})p^{21}_{\mathbf{k}}. \tag{5}$$

Using the semiconductor Boltzmann collision rate

$$\frac{d}{dt}f^{i}_{\mathbf{k}}|_{\mathrm{corr}} = -f^{i}_{\mathbf{k}}\Gamma^{i,\mathrm{out}}_{\mathrm{d}} + (1-f^{i}_{\mathbf{k}})\Gamma^{i,\mathrm{in}}_{\mathrm{d}}, \tag{6}$$

we can identify the inverse of the diagonal damping rate Γ_{d} in the polarization dynamics with the T_2 time known from two-level atomic systems,[1] i.e., $(\Gamma_{\mathrm{d}})^{-1} = T_2$. The nondiagonal terms yield a momentum dependent *nondiagonal damping*. As will be shown in the following section, the nondiagonal correlation contributions play a significant role for the homogeneous width of the IS absorption line since they compensate strongly for the diagonal counterparts, even more strongly than for the interband case.[2]

IV. THEORETICAL RESULTS

For the numerical simulations we use a square-well potential model with a barrier height of $V_0 = 350$ meV and consider small signal absorption and quasiequilibrium conditions, i.e., we describe the electron distribution $f^{1}_{\mathbf{k}} = \langle a^{\dagger}_{\mathbf{k}1} a_{\mathbf{k}1}\rangle$ by a Fermi-Dirac distribution for a given carrier density and temperature and assume $f^{2}_{\mathbf{k}} = 0$. Furthermore, we assume that the phonons can be treated as a bath for the dynamical electronic system. Thus we describe the phonon distribution $n_{\mathbf{q}}$ by a thermal Bose function.

As we will show in the following, the line shapes and line widths of IS absorption spectra are due to (i) carrier-carrier and carrier-phonon interactions (strongly dependent on the three-dimensional character of the Coulomb and Fröhlich matrix elements), (ii) different effective masses, and (iii) radiative interaction with the transverse field. We examine the influence of these contributions and their interplay by focusing on them separately. Note that the mean-field contributions are included in all calculations.

First, we assume the same effective mass for both subbands ($m_1 = m_2 = 0.0665 m_0$), i.e., the energy difference between states $\mathbf{k}$ in each subband

$$\epsilon^{2}_{\mathbf{k}} - \epsilon^{1}_{\mathbf{k}} = \mathrm{const}, \tag{7}$$

and consider only a single quantum well of the MQW sample described above. By considering a single quantum well, we exclude the impact of radiative interaction with the transverse field on the line shape of the absorption spectrum. We thus investigate the influence of pure carrier-carrier and carrier-phonon interactions. Considering the Coulomb and Fröhlich formfactors [cf. Eq. (B2)]

$$\mathcal{F}^{abcd}_{\mathbf{q}} = \int dz \zeta^{*}_{a}(z)\zeta_{c}(z)\int dz' \zeta^{*}_{b}(z')\zeta_{d}(z')e^{-|\mathbf{q}||z-z'|},$$

$$\mathcal{F}^{ab}_{Q_\perp} = \int dz \zeta^{*}_{a}(z)\zeta_{b}(z)e^{iQ_\perp z}, \tag{8}$$

we see that in the limit

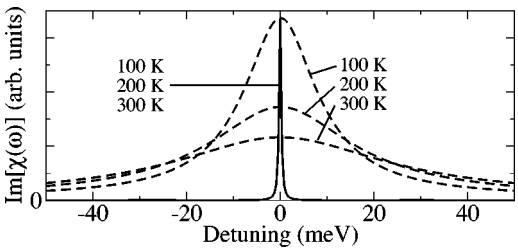

FIG. 3. Im$[\chi(\omega)]$ of a single quantum well with the same effective mass for both subbands for different temperatures—calculated by approximating the Coulomb and Fröhlich matrix elements by Eq. (10). The spectra are that of noninteracting single-particle excitations (solid curve, scaled in height). Neglecting the nondiagonal contributions (dashed curves) yields a strong overestimation of the linewidth.

$$e^{-|\mathbf{q}||z-z'|}\approx 1 \quad \text{and} \quad e^{iQ_\perp z}\approx 1, \tag{9}$$

the intersubband formfactors vanish and the intrasubband formfactors all have the same value:

$$\mathcal{F}_{\mathbf{q}}^{abcd}\approx \delta_{a,c}\delta_{b,d}, \quad \mathcal{F}_{Q_\perp}^{ab}\approx \delta_{a,b}. \tag{10}$$

If we approximate the matrix elements using Eq. (10), we neglect the three-dimensional character of the matrix elements. Taking the sum over all **k** contributions one can show by renumbering the summation indices in Eqs. (B3a)–(B5) that in this case the total contribution of the Coulomb interaction among the carriers and the total contribution of the electron-phonon interaction to the macroscopic polarization vanish. Thus the linear susceptibility $\chi(\omega)$, extracted from the IS coherence, is that of noninteracting single-particle excitations, Im$[\chi(\omega)]\propto\delta(\omega-\omega_0)$ (see the solid curve in Fig. 3) and does not show a dependence on temperature. This result can be compared to that of Kohn's Theorem[22] which states that, for a parabolic potential or in the presence of a magnetic field, the absorption is independent of the electron-electron interaction. Note that, in contrast to Kohn's Theorem which is valid for all strengths of the parabolic potential and for all carrier densities, the approximation for the formfactors used above is justified only for $(-|\mathbf{q}||z-z'|)\approx 0$ and $(iQ_\perp z)\approx 0$, i.e., in the limit of thin wells and low densities.[7] If we neglect the nondiagonal correlation contributions $\Xi_{\mathrm{nd}}(p^{21}_{\mathbf{k}+\mathbf{k}''})$ and consider only the diagonal terms $\Xi_{\mathrm{d}}(p^{21}_{\mathbf{k}})$, i.e., if we approximate the correlation contributions by the inverse of the T_2 time, the spectra show a strong temperature-dependent broadening (dashed curves in Fig. 3). This demonstrates clearly the cancellation effects between diagonal and nondiagonal terms. *Disregarding the nondiagonal terms completely neglects possible interference effects between various scattering events and yields a strong overestimation of the linewidth.*

Next, we include the three-dimensional character of the matrix elements by using Eq. (8) instead of Eq. (10) (Fig. 4). In contrast to the δ-function behavior of the solid curve in Fig. 3, we now observe spectra which are slightly asymmetric towards the short-wavelength side and have a finite linewidth. The linewidth is temperature dependent and originates only from the three-dimensional character of the matrix elements. The main contribution to the linewidth stems from the lifetime of the electron in subband 2, which in turn is determined mostly by emission (and absorption at higher temperatures) of LO phonons.

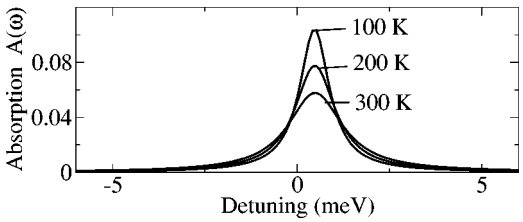

FIG. 4. Calculated absorption $A(\omega)$ of a single quantum well with cc-/cp-correlation contributions assuming equal masses showing the influence of pure electron-electron and electron-phonon interactions.

From now on, we additionally consider the different effective masses of the subbands due to the conduction band nonparabolicity in the form of the in-plane effective-mass scheme proposed by Ekenberg,[4,23] i.e., we assume that the subbands themselves have parabolic curvatures but different effective masses ($m_2=0.088m_0$ and $m_1=0.071m_0$), which is a good approximation for low densities where only states with small in-plane momenta **k** are occupied. To obtain an impression of the influence of the difference in the masses on the spectra, we first include only the different masses as a dephasing contribution (Fig. 5): we neglect dephasing due to carrier-carrier and carrier-phonon scattering, i.e., $(d/dt)p^{21}_{\mathbf{k}}|_{\mathrm{corr}}=0$. The finite linewidth and the line shape is thus due to (i) the different masses of the two subbands [inhomogeneous broadening, Fig. 1(b)] and (ii) its interaction with the mean-field effects, $(d/dt)p^{21}_{\mathbf{k}}|_{\mathrm{MF}}$, only. The spectra are very asymmetric, they show a pronounced tail towards the long-wavelength side. Note that due to the small carrier density considered here, the depolarization (identical to the interaction with the longitudinal field) compensates the effects of the different effective masses[6] only to a small extent.

Finally, we compute absorption spectra considering both different effective masses and carrier-carrier and carrier-phonon correlation contributions (Fig. 6). Even for the small carrier density considered here, radiative interaction affects the linewidth of the spectra. To compare with experimental results, we now consider the whole multiple quantum well system in the geometry described above. Thus, the spectra are the result of the simultaneous inclusion of (i) carrier-

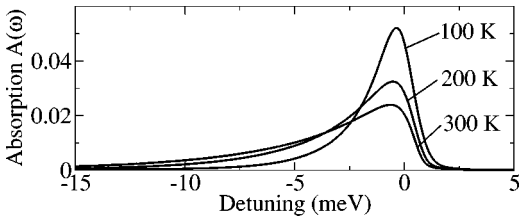

FIG. 5. Calculated $A(\omega)$ of a single quantum well with different effective masses but without inclusion of cc-/cp-correlation contributions showing the dephasing due to the different subband masses [Fig. 1(b)].

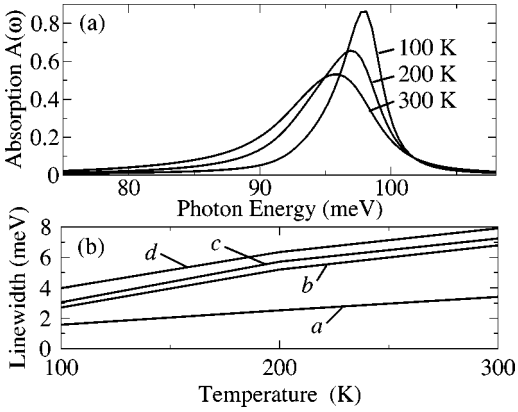

FIG. 6. (a) Simultaneous inclusion of cc-/cp-correlation contributions and different effective masses of the MQW sample. (b) Comparison of the linewidth with regard to different dephasing contributions: linewidth of a single quantum well with (*a*) only cc correlations, (*b*) only cp correlations, (*c*) cc and cp correlations; (*d*) linewidth of full theory, i.e., with radiative interaction.

carrier and carrier-phonon interactions (including the three-dimensional character of the matrix elements), (ii) the different effective masses, and (iii) radiative interaction with the transverse field. The absorption lines are almost Lorentzian-like. With increasing temperature, the absorption peak shifts ($\approx$3 meV between 100 and 300 K) to lower energies. As stated before, the nondiagonal correlation contributions have the effect of compensating the diagonal ones to a large extent. Neglecting the nondiagonal correlation contributions in this case, the linewidth varies between 20 meV at 100 K and 50 meV at 300 K (not shown). Comparing the broadening due to the different dephasing contributions [Fig. 6(b)], we see that carrier-carrier and carrier-phonon interactions are nonadditive dephasing mechanisms, due to interference effects of the diagonal and nondiagonal correlation contributions. This observation is similar to that made for energy-relaxation processes in quantum-cascade lasers.[24] Note that the strength of these interference effects depends on both carrier density and the difference in the effective masses. Comparing the linewidth including cc and cp correlations of a single quantum well only (curve *c*) and all 51 wells (curve *d*), we find that even for the moderate density considered here, radiative damping leads to an additional broadening of $\Delta E_{\mathrm{rad}} \approx 1$ meV, which is about 12% (at 300 K) to 25% (at 100 K) of the final linewidth.

V. COMPARISON WITH EXPERIMENTAL RESULTS

In Fig. 7 we present intersubband absorption measurements on the MQW sample described in Sec. II at three different temperatures. One can clearly see the nearly symmetric IS absorption line around 100 meV. With increasing temperature one observes a shift towards lower energy, a decrease of the amplitude, and an increase of the linewidth. As can be seen in direct comparison with the theoretical results [Figs. 5 and 6(a)], only the full calculation [Fig. 6(a)] yields satisfactory agreement with the experiment (line shape, linewidth, peak position, and height). For this sample,

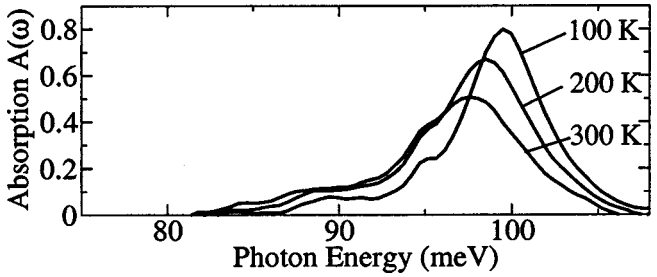

FIG. 7. Measured IS absorption $A(\omega)$ spectra on the MQW sample as explained in the text.

at low temperatures the linewidth is determined to approximately equal amounts by the lifetime in subband 2, by intrasubband scattering processes, and by the radiative coupling.

Due to the fact that the random-phase approximation (RPA) used in the derivation of the equation of motion for the intersubband coherence is valid in the low-density regime only for high temperatures,[25] we expect the calculation of the absorption to fail for low temperatures. An indication of this can already be seen in Figs. 6(a) and 7, where the agreement between experiment and theory is better at the elevated temperatures 200 and 300 K, than at the lower temperature of 100 K.

VI. CONCLUSION

In conclusion, we have presented a microscopic many-particle theory for the dephasing of coherent intersubband excitations in semiconductor quantum wells including carrier-carrier, carrier-phonon scattering, and light propagation effects. By including first the different dephasing mechanisms separately and then simultaneously, we investigated their complex interplay. Furthermore, we analyzed the impact of nondiagonal correlation contributions on absorption spectra. Excellent agreement with experimental results is obtained by the full theory. It is shown that no single process is dominating, thus making it necessary to consider all contributions simultaneously.

ACKNOWLEDGMENTS

We acknowledge discussions with Stephan W. Koch and financial support by the ''Berliner Programm zur Förderung von Frauen in Forschung und Lehre'' and by the Deutsche Forschungsgemeinschaft through Forschergruppe 394.

APPENDIX A: LOCAL FIELD

In order to include radiative interaction in the calculation of IS absorption spectra, we determine the local field $\mathbf{E}^{(n)}(z,\omega)$ in the geometry considered (Fig. 2) using a nonlocal Green's-function formalism.[10,16] Without the medium-1/medium-2 interface each sheet of polarization at a given z would produce—besides the local contribution—a leftward and a rightward wave. Since in the geometry considered here, the interface is located on the right side of the MQW system (Fig. 2), the interface does not affect the leftward wave and we find the local field in quantum well n to consist

of (i) the incident field, (ii) the reflection of the incident field at the interface, (iii) the local contribution, (iv) rightward-wave contributions from all planes $z'<z$, (v) directly generated leftward waves from all planes $z'>z$, and (vi) leftward-wave contributions from the reflection of all rightward waves at the interface. Contributions (iii)–(vi) are due to the polarizations in the quantum wells:

$$\mathbf{E}^{(n)}(z,\omega)=E_{\mathrm{in}}(\hat{\mathbf{p}}_+e^{iq_\perp z}+r_{12}^p\hat{\mathbf{p}}_-e^{-iq_\perp z}) + \sum_{m=1}^{N}\int_{(m)}dz'\,\vec{\vec{\mathcal{G}}}_{z,z'}^{0,R}(\omega)\mathbf{P}^{(m)}(z',\omega). \quad \text{(A1)}$$

Here the incident wave is assumed to be a *p*-polarized plane wave and r_{12}^p is the corresponding Fresnel coefficient. $\vec{\vec{\mathcal{G}}}_{z,z'}^{0,R}(\omega)$ denotes the retarded Green's-function tensor in dyadic form with regard to total reflection at the medium-1/medium-2 interface[19]

$$\vec{\vec{\mathcal{G}}}_{z,z'}^{0,R}(\omega)=-\mu_0\omega^2\left\{\frac{\delta(z-z')}{\omega^2\varepsilon_\infty\mu_0}\hat{\mathbf{z}}\hat{\mathbf{z}}+\frac{e^{iq_\perp|z-z'|}}{2iq_\perp}[(-\hat{\mathbf{y}}\hat{\mathbf{y}} + \hat{\mathbf{p}}_+\hat{\mathbf{p}}_+)\Theta(z-z')+(-\hat{\mathbf{y}}\hat{\mathbf{y}}+\hat{\mathbf{p}}_-\hat{\mathbf{p}}_-)\Theta(z'-z)] + \frac{e^{-iq_\perp(z+z')}}{2iq_\perp}r_{12}^p\hat{\mathbf{p}}_+\hat{\mathbf{p}}_-\right\}, \quad \text{(A2)}$$

where $\hat{\mathbf{p}}_\pm=(\mp q_\perp\hat{\mathbf{x}}+q_{||}\hat{\mathbf{z}})/q$ and $\mathbf{q}_\pm=q_{||}\hat{\mathbf{x}}\pm q_\perp\hat{\mathbf{z}}$ are the relevant vectors. The wave-vector projections perpendicular and parallel to the well layers are given by $q_\perp=\omega\sqrt{\varepsilon_\infty\mu_0}\cos\theta$ and $q_{||}=\omega\sqrt{\varepsilon_\infty\mu_0}\sin\theta$. ε_∞ denotes the optical background permittivity, μ_0 the permeability of free space, Θ the Heaviside unit step function, and δ the Dirac δ function. To obtain the absorption, $A(\omega)=1-|\mathbf{E}_{\mathrm{out}}(\omega)|^2/|\mathbf{E}_{\mathrm{in}}(\omega)|^2$, we insert Eq. (A2) and Eq. (1b) in Eq. (A1) and let the observation point z be located in space ($z<0$) which yields the outgoing (leftward) field

$$\mathbf{E}^{\mathrm{out}}(z,\omega)=e^{-iq_\perp z}\left\{r_{12}^p\mathbf{E}_{\mathrm{in}}\hat{\mathbf{p}}_- - \frac{\mu_0\omega^2}{2iq_\perp}\sum_{m=1}^{N}\int\int_{(m)}dz' \times dz''[e^{iq_\perp z'}(-\hat{\mathbf{y}}\hat{\mathbf{y}}+\hat{\mathbf{p}}_-\hat{\mathbf{p}}_-)+e^{-iq_\perp z'}r_{12}^p\hat{\mathbf{p}}_+\hat{\mathbf{p}}_-] \times\vec{\vec{\chi}}_{z',z''}^{(m)}(\omega)\cdot\mathbf{E}^{(m)}(z'',\omega)\right\}. \quad \text{(A3)}$$

APPENDIX B: IS COHERENCE

To determine the IS coherence $p_{\mathbf{k}}^{21}(\omega)$, which yields the dipole density $\mathbf{P}^{(n)}(z,\omega)$, the source of the electromagnetic emission in quantum well *n* [cf. Eq. (1a)], we need to consider the system Hamiltonian.

In our model, the total Hamiltonian in second quantization is given by $H=H_0+H_{\mathrm{cf}}+H_{\mathrm{cc}}+H_{\mathrm{cp}}$, where the Hamiltonian of the noninteracting Bloch electrons and phonons is represented by H_0, the field-carrier interaction by H_{cf}, the Coulomb interaction of the electronic system by H_{cc}, and the electron-phonon interaction by H_{cp}:

$$H_0=\sum_{a,\mathbf{k}}\epsilon_{\mathbf{k}}^a a_{a\mathbf{k}}^\dagger a_{a\mathbf{k}}+\sum_{\mathbf{Q}}\hbar\omega_{\mathrm{LO}}b_{\mathbf{Q}}^\dagger b_{\mathbf{Q}}, \quad \text{(B1a)}$$

$$H_{\mathrm{cf}}=\sum_{a,b,\mathbf{k}}\int dz\,\mathbf{d}_{ab}(z)\cdot\mathbf{E}(z,t)a_{a\mathbf{k}}^\dagger a_{b\mathbf{k}}, \quad \text{(B1b)}$$

$$H_{\mathrm{cc}}=\frac{1}{2}\sum_{abcd}\sum_{\mathbf{k},\mathbf{k}',\mathbf{q}}\hat{V}_{\mathbf{q}}^{abcd}a_{a\mathbf{k}+\mathbf{q}}^\dagger a_{b\mathbf{k}'-\mathbf{q}}^\dagger a_{d\mathbf{k}'}a_{c\mathbf{k}}, \quad \text{(B1c)}$$

$$H_{\mathrm{cp}}=\sum_{a,b,\mathbf{k}}\sum_{\mathbf{Q}}[\hat{g}_{\mathbf{Q}}^{ab}a_{a\mathbf{k}}^\dagger b_{\mathbf{Q}}a_{b\mathbf{k}-\mathbf{Q}_{||}}+\mathrm{H.a.}]. \quad \text{(B1d)}$$

In Eqs. (B1a)–(B1d) the indices *a*, *b*, *c*, and *d* are subband indices, $\mathbf{k}$, $\mathbf{k}'$, and $\mathbf{q}$ denote 2D electron wave vectors, and $\mathbf{Q}$ is the 3D phonon wave vector. $\epsilon_{a\mathbf{k}}$ denotes the energy of an electron in subband *a* with wave vector $\mathbf{k}$, $\hbar\omega_{\mathrm{LO}}$ the LO phonon energy, $b_{\mathbf{Q}}^\dagger(b_{\mathbf{Q}})$ the creation (annihilation) operator for a phonon with the 3D wave vector $\mathbf{Q}$. The unscreened Coulomb and Fröhlich coupling matrix elements are given by

$$\hat{V}_{\mathbf{q}}^{abcd}=V_{\mathbf{q}}^{abcd}\delta_{s_{\mathbf{q}},0}=\frac{e^2}{2\varepsilon_s\mathcal{A}}\frac{\mathcal{F}_{\mathbf{q}}^{abcd}}{|\mathbf{q}|}, \quad \text{(B2)}$$

$$\mathcal{F}_{\mathbf{q}}^{abcd}=\int dz\,\zeta_a^*(z)\zeta_c(z)\int dz'\,\zeta_b^*(z')\zeta_d(z')e^{-|\mathbf{q}||z-z'|},$$

$$\hat{g}_{\mathbf{Q}}^{ab}=g_{\mathbf{Q}}^{ab}\delta_{s_{\mathbf{Q}},0}=-i\sqrt{\frac{e^2\hbar\omega_{\mathrm{LO}}}{2\mathcal{V}}\left(\frac{1}{\varepsilon_\infty}-\frac{1}{\varepsilon_s}\right)}\frac{\mathcal{F}_{Q_\perp}^{ab}}{|\mathbf{Q}|},$$

$$\mathcal{F}_{Q_\perp}^{ab}=\int dz\,\zeta_a^*(z)\zeta_b(z)e^{iQ_\perp z}.$$

Here, $\mathcal{V}=\mathcal{A}L$ denotes the normalization volume, ζ_i is the envelope function in the confined direction, ε_s denotes the static and ε_∞ the optical dielectric permittivity.

Using the Robertson equation[20] to derive the equation of motion for the intersubband coherence, the free-carrier and carrier-field contributions, i.e., the contributions due to H_0 and H_{cf}, are easily obtained as

$$\frac{d}{dt}p_{\mathbf{k}}^{21}|_{0,\mathrm{cf}}=\frac{i}{\hbar}(\epsilon_{\mathbf{k}}^2-\epsilon_{\mathbf{k}}^1)p_{\mathbf{k}}^{21} \quad \text{(B3a)}$$

$$+\frac{i}{\hbar}\int dz\mathbf{E}(z,t)\cdot\mathbf{d}_{21}(z)[f_{\mathbf{k}}^2-f_{\mathbf{k}}^1]. \quad \text{(B3b)}$$

They consist of the transition energy, Eq. (B3a), and the electric-dipole interaction energy, Eq. (B3b). $f_{\mathbf{k}}^i=\langle a_{i\mathbf{k}}^\dagger a_{i\mathbf{k}}\rangle$ denotes the electron distribution. The inclusion of the carrier-carrier [Eq. (B1c)] and carrier-phonon [Eq. (B1d)] interactions yields an infinite hierarchy involving higher-order density matrices. Similar to Ref. 18, we use a correlation expansion to truncate this hierarchy. We start with the carrier-carrier interaction and factorize the two-particle density matrices into single-particle density matrices[1,18] which yields the *first-order* or *mean-field contributions*:

$$\frac{d}{dt}p_{\mathbf{k}}^{21}|_{\mathrm{MF}}=\frac{i}{\hbar}\sum_{\mathbf{q}\neq 0}(V_{\mathbf{q}}^{2112}-V_{\mathbf{q}}^{2222})f_{\mathbf{k}-\mathbf{q}}^{2}p_{\mathbf{k}}^{21} \tag{B4a}$$

$$-\frac{i}{\hbar}\sum_{\mathbf{q}\neq 0}(V_{\mathbf{q}}^{2112}-V_{\mathbf{q}}^{1111})f_{\mathbf{k}-\mathbf{q}}^{1}p_{\mathbf{k}}^{21} \tag{B4b}$$

$$+\frac{i}{\hbar}\sum_{\mathbf{q}\neq 0}V_{\mathbf{q}}^{1212}p_{\mathbf{k}-\mathbf{q}}^{21}[f_{\mathbf{k}}^{2}-f_{\mathbf{k}}^{1}] \tag{B4c}$$

$$-2\frac{i}{\hbar}\sum_{\mathbf{q}\neq 0}V_{0}^{2112}p_{\mathbf{q}}^{21}[f_{\mathbf{k}}^{2}-f_{\mathbf{k}}^{1}]. \tag{B4d}$$

This lowest order of the hierarchy contains the exchange self-energy, Eqs. (B4a) and (B4b), the excitonic contribution, Eq. (B4c), and the depolarization effect, Eq. (B4d), which renormalize the free-carrier and carrier-field contributions. These contributions and their interplay have been investigated quite thoroughly in Refs. 6–9 and 26. We therefore refer the reader to these papers. Note that, because in our approach the response to the total (longitudinal and transverse) classical field is calculated, the depolarization contribution (identical with the longitudinal field) must not be included in the material equation of motion [Eq. (3)], otherwise this effect would be counted twice. Next we include the carrier-phonon interaction, where we assume that we can treat the phonons as a bath for the dynamical electronic system. As has been shown in Ref. 19, the first-order contributions of the carrier-phonon interaction, which are obtained by factorizing the phonon-assisted density matrices without considering correlations between carriers and phonons, vanish for the phonon bath considered here. The next order in the hierarchy is obtained by including the derivations from the factorization of the two-particle density matrices and the phonon-assisted density matrices, respectively.[19] This yields the *second-order* or *correlation contributions*

$$\frac{d}{dt}p_{\mathbf{k}}^{21}|_{\mathrm{corr}}=-\frac{\pi}{\hbar}\Xi_{\mathrm{d}}(p_{\mathbf{k}}^{21})+\frac{\pi}{\hbar}\sum_{\mathbf{k}''}\Xi_{\mathrm{nd}}(p_{\mathbf{k}+\mathbf{k}''}^{21}), \tag{B5}$$

which can be decomposed into diagonal terms dependent on the IS coherence $p_{\mathbf{k}}^{21}$ and nondiagonal terms, which couple IS coherences at different wave vectors. In the following we use the Markovian and second-order Born approximation and keep only terms that are linear in the IS coherence. With these approximations the diagonal part of the correlation contribution is given as the sum of the effects of carrier-phonon scattering and of carrier-carrier scattering

$$\Xi_{\mathrm{d}}(p_{\mathbf{k}}^{21})=\Gamma_{\mathrm{d}}p_{\mathbf{k}}^{21}=\frac{1}{2}\sum_{i=1,2}(\Gamma_{\mathrm{d}}^{i,\mathrm{cp}}+\Gamma_{\mathrm{d}}^{i,\mathrm{cc}})p_{\mathbf{k}}^{21}, \tag{B6}$$

with

$$\begin{aligned}\Gamma_{\mathrm{d}}^{1,\mathrm{cp}}=2\sum_{\mathbf{Q}}\{&\delta(-\epsilon_{\mathbf{k}}^{1}+\epsilon_{\mathbf{k}+\mathbf{Q}_{||}}^{1}-\hbar\omega_{\mathrm{LO}})|g_{\mathbf{Q}}^{11}|^{2}\{n_{\mathbf{Q}}(1-f_{\mathbf{k}+\mathbf{Q}_{||}}^{1})\\&+(n_{\mathbf{Q}}+1)f_{\mathbf{k}+\mathbf{Q}_{||}}^{1}\}+\delta(-\epsilon_{\mathbf{k}}^{1}+\epsilon_{\mathbf{k}+\mathbf{Q}_{||}}^{1}+\hbar\omega_{\mathrm{LO}})|g_{\mathbf{Q}}^{11}|^{2}\\&\times\{(n_{\mathbf{Q}}+1)(1-f_{\mathbf{k}+\mathbf{Q}_{||}}^{1})+n_{\mathbf{Q}}f_{\mathbf{k}+\mathbf{Q}_{||}}^{1}\}\\&+\delta(-\epsilon_{\mathbf{k}}^{2}+\epsilon_{\mathbf{k}+\mathbf{Q}_{||}}^{1}-\hbar\omega_{\mathrm{LO}})|g_{\mathbf{Q}}^{12}|^{2}\{n_{\mathbf{Q}}(1-f_{\mathbf{k}+\mathbf{Q}_{||}}^{1})\\&+(n_{\mathbf{Q}}+1)f_{\mathbf{k}+\mathbf{Q}_{||}}^{1}\}+\delta(-\epsilon_{\mathbf{k}}^{2}+\epsilon_{\mathbf{k}+\mathbf{Q}_{||}}^{1}+\hbar\omega_{\mathrm{LO}})|g_{\mathbf{Q}}^{12}|^{2}\\&\times\{(n_{\mathbf{Q}}+1)(1-f_{\mathbf{k}+\mathbf{Q}_{||}}^{1})+n_{\mathbf{Q}}f_{\mathbf{k}+\mathbf{Q}_{||}}^{1}\}],\end{aligned}$$

$$\begin{aligned}\Gamma_{\mathrm{d}}^{1,\mathrm{cc}}=2\sum_{\mathbf{k}',\mathbf{q}}\{&\delta(\epsilon_{\mathbf{k}}^{1}+\epsilon_{\mathbf{k}'}^{1}-\epsilon_{\mathbf{k}'-\mathbf{q}}^{1}-\epsilon_{\mathbf{k}+\mathbf{q}}^{1})V_{\mathbf{q}}^{1111}(2V_{\mathbf{q}}^{1111}\\&-V_{\mathbf{k}'-\mathbf{k}-\mathbf{q}}^{1111})\{f_{\mathbf{k}'}^{1}(1-f_{\mathbf{k}'-\mathbf{q}}^{1})(1-f_{\mathbf{k}+\mathbf{q}}^{1})\\&+f_{\mathbf{k}'-\mathbf{q}}^{1}f_{\mathbf{k}+\mathbf{q}}^{1}(1-f_{\mathbf{k}'}^{1})\}+\delta(\epsilon_{\mathbf{k}}^{1}+\epsilon_{\mathbf{k}'}^{1}-\epsilon_{\mathbf{k}'-\mathbf{q}}^{2}-\epsilon_{\mathbf{k}+\mathbf{q}}^{2})\\&\times V_{\mathbf{q}}^{1122}(2V_{\mathbf{q}}^{1122}-V_{\mathbf{k}'-\mathbf{k}-\mathbf{q}}^{1122})\{f_{\mathbf{k}'}^{1}(1-f_{\mathbf{k}'-\mathbf{q}}^{2})(1-f_{\mathbf{k}+\mathbf{q}}^{2})\\&+f_{\mathbf{k}'-\mathbf{q}}^{2}f_{\mathbf{k}+\mathbf{q}}^{2}(1-f_{\mathbf{k}'}^{1})\}+\delta(\epsilon_{\mathbf{k}}^{1}+\epsilon_{\mathbf{k}'}^{2}-\epsilon_{\mathbf{k}'-\mathbf{q}}^{1}-\epsilon_{\mathbf{k}+\mathbf{q}}^{2})\\&\times V_{\mathbf{q}}^{1221}(2V_{\mathbf{q}}^{1221}-V_{\mathbf{k}'-\mathbf{k}-\mathbf{q}}^{1212})\{f_{\mathbf{k}'}^{2}(1-f_{\mathbf{k}'-\mathbf{q}}^{1})(1-f_{\mathbf{k}+\mathbf{q}}^{2})\\&+f_{\mathbf{k}'-\mathbf{q}}^{1}f_{\mathbf{k}+\mathbf{q}}^{2}(1-f_{\mathbf{k}'}^{2})\}+\delta(\epsilon_{\mathbf{k}}^{1}+\epsilon_{\mathbf{k}'}^{2}-\epsilon_{\mathbf{k}'-\mathbf{q}}^{2}-\epsilon_{\mathbf{k}+\mathbf{q}}^{1})\\&\times V_{\mathbf{q}}^{1212}(2V_{\mathbf{q}}^{1212}-V_{\mathbf{k}'-\mathbf{k}-\mathbf{q}}^{1221})\{f_{\mathbf{k}'}^{2}(1-f_{\mathbf{k}'-\mathbf{q}}^{2})(1-f_{\mathbf{k}+\mathbf{q}}^{1})\\&+f_{\mathbf{k}'-\mathbf{q}}^{2}f_{\mathbf{k}+\mathbf{q}}^{1}(1-f_{\mathbf{k}'}^{2})\}].\end{aligned}$$

Here and in the next equation we give only the terms for subband $i=1$, the terms for $i=2$ are obtained by exchanging the subband indices 1 and 2.

The nondiagonal part of the correlation contribution consists of the following terms:

$$\begin{aligned}\sum_{\mathbf{k}''}\Xi_{\mathrm{nd}}(p_{\mathbf{k}+\mathbf{k}''}^{21})=\sum_{i=1,2}\Bigg[&\sum_{\mathbf{Q}}\Gamma_{\mathrm{nd}}^{i,\mathrm{cp}}p_{\mathbf{k}+\mathbf{Q}_{||}}^{21}+\sum_{\mathbf{k}',\mathbf{q}}\Gamma_{\mathrm{nd1}}^{i,\mathrm{cc}}p_{\mathbf{k}'-\mathbf{q}}^{21}\\&+\sum_{\mathbf{q}}\Gamma_{\mathrm{nd2}}^{i,\mathrm{cc}}p_{\mathbf{k}+\mathbf{q}}^{21}-\sum_{\mathbf{k}'}\Gamma_{\mathrm{nd3}}^{i,\mathrm{cc}}p_{\mathbf{k}'}^{21}\Bigg]\end{aligned} \tag{B7}$$

with the abbreviations

$$\begin{aligned}\Gamma_{\mathrm{nd}}^{1,\mathrm{cp}}=&\delta(-\epsilon_{\mathbf{k}}^{1}+\epsilon_{\mathbf{k}+\mathbf{Q}_{||}}^{1}-\hbar\omega_{\mathrm{LO}})g_{\mathbf{Q}_{||}}^{11*}g_{\mathbf{Q}_{||}}^{22}\{(n_{\mathbf{Q}_{||}}+1)(1-f_{\mathbf{k}}^{1})\\&+n_{\mathbf{Q}_{||}}f_{\mathbf{k}}^{1}\}+\delta(-\epsilon_{\mathbf{k}}^{1}+\epsilon_{\mathbf{k}+\mathbf{Q}_{||}}^{1}+\hbar\omega_{\mathrm{LO}})g_{\mathbf{Q}_{||}}^{11*}g_{\mathbf{Q}_{||}}^{22}\\&\times\{n_{\mathbf{Q}_{||}}(1-f_{\mathbf{k}}^{1})+(n_{\mathbf{Q}_{||}}+1)f_{\mathbf{k}}^{1}\},\end{aligned}$$

$$\begin{aligned}\Gamma_{\mathrm{nd1}}^{1,\mathrm{cc}}=&\delta(\epsilon_{\mathbf{k}}^{1}+\epsilon_{\mathbf{k}'}^{2}-\epsilon_{\mathbf{k}'-\mathbf{q}}^{1}-\epsilon_{\mathbf{k}+\mathbf{q}}^{2})V_{\mathbf{q}}^{2222}(2V_{\mathbf{q}}^{1221}-V_{\mathbf{k}'-\mathbf{k}-\mathbf{q}}^{1212})\\&\times\{f_{\mathbf{k}+\mathbf{q}}^{2}(1-f_{\mathbf{k}}^{1})(1-f_{\mathbf{k}'}^{2})+f_{\mathbf{k}}^{1}f_{\mathbf{k}'}^{2}(1-f_{\mathbf{k}+\mathbf{q}}^{2})\}\\&+\delta(\epsilon_{\mathbf{k}}^{1}+\epsilon_{\mathbf{k}'}^{1}-\epsilon_{\mathbf{k}'-\mathbf{q}}^{1}-\epsilon_{\mathbf{k}+\mathbf{q}}^{1})V_{\mathbf{q}}^{1221}(2V_{\mathbf{q}}^{1111}-V_{\mathbf{k}'-\mathbf{k}-\mathbf{q}}^{1111})\\&\times\{f_{\mathbf{k}+\mathbf{q}}^{1}(1-f_{\mathbf{k}}^{1})(1-f_{\mathbf{k}'}^{1})+f_{\mathbf{k}}^{1}f_{\mathbf{k}'}^{1}(1-f_{\mathbf{k}+\mathbf{q}}^{1})\},\end{aligned}$$

$$\Gamma^{1,cc}_{nd2}=\sum_{\mathbf{k}'}[\delta(\epsilon^1_{\mathbf{k}}+\epsilon^2_{\mathbf{k}'}-\epsilon^2_{\mathbf{k}'-\mathbf{q}}-\epsilon^1_{\mathbf{k}+\mathbf{q}})\times V^{2222}_{\mathbf{q}}(2V^{1212}_{\mathbf{q}}-V^{1221}_{\mathbf{k}'-\mathbf{k}-\mathbf{q}})\{f^2_{\mathbf{k}'-\mathbf{q}}(1-f^1_{\mathbf{k}})(1-f^2_{\mathbf{k}'})+f^1_{\mathbf{k}}f^2_{\mathbf{k}'}(1-f^2_{\mathbf{k}'-\mathbf{q}})\}+\delta(\epsilon^1_{\mathbf{k}}+\epsilon^1_{\mathbf{k}'}-\epsilon^1_{\mathbf{k}'-\mathbf{q}}-\epsilon^1_{\mathbf{k}+\mathbf{q}})\times V^{2121}_{\mathbf{q}}(2V^{1111}_{\mathbf{q}}-V^{1111}_{\mathbf{k}'-\mathbf{k}-\mathbf{q}})\{f^1_{\mathbf{k}'-\mathbf{q}}(1-f^1_{\mathbf{k}})(1-f^1_{\mathbf{k}'})+f^1_{\mathbf{k}}f^1_{\mathbf{k}'}(1-f^1_{\mathbf{k}'-\mathbf{q}})\}],$$

$$\Gamma^{1,cc}_{nd3}=\sum_{\mathbf{q}}[\delta(\epsilon^1_{\mathbf{k}}+\epsilon^2_{\mathbf{k}'}-\epsilon^2_{\mathbf{k}'-\mathbf{q}}-\epsilon^1_{\mathbf{k}+\mathbf{q}})\times V^{1221}_{\mathbf{q}}(2V^{1212}_{\mathbf{q}}-V^{1221}_{\mathbf{k}'-\mathbf{k}-\mathbf{q}})\{f^1_{\mathbf{k}}(1-f^2_{\mathbf{k}'-\mathbf{q}})(1-f^1_{\mathbf{k}+\mathbf{q}})+f^2_{\mathbf{k}'-\mathbf{q}}f^1_{\mathbf{k}+\mathbf{q}}(1-f^1_{\mathbf{k}})\}+\delta(\epsilon^1_{\mathbf{k}}+\epsilon^2_{\mathbf{k}'}-\epsilon^1_{\mathbf{k}'-\mathbf{q}}-\epsilon^2_{\mathbf{k}+\mathbf{q}})\times V^{1212}_{\mathbf{q}}(2V^{1221}_{\mathbf{q}}-V^{1212}_{\mathbf{k}'-\mathbf{k}-\mathbf{q}})\{f^1_{\mathbf{k}}(1-f^1_{\mathbf{k}'-\mathbf{q}})(1-f^2_{\mathbf{k}+\mathbf{q}})+f^1_{\mathbf{k}'-\mathbf{q}}f^2_{\mathbf{k}+\mathbf{q}}(1-f^1_{\mathbf{k}})\}].$$

Note that in contrast to Eqs. (1a) and (B1), where the sum over the spin indices is absorbed in the sum over the wave vectors, in Eqs. (B4) and (B5) the summations over the spin indices have already been performed and thus only the wave vector **k** includes a spin index.

We include the effect of screening on the electron-electron Coulomb interaction in the following manner. For interactions which involve only intrasubband transitions, i.e., interactions represented by $V^{1111}_{\mathbf{q}}$, $V^{2222}_{\mathbf{q}}$, and $V^{1212}_{\mathbf{q}}=V^{2121}_{\mathbf{q}}$, we replace the unscreened Coulomb interaction $V^{iiii}_{\mathbf{q}}$ and $V^{ijij}_{\mathbf{q}}$ with

$$\frac{V^{iiii}_{\mathbf{q}}+\mathcal{V}^2_{\mathbf{q}}\Pi^{jj}}{D} \quad \text{and} \quad \frac{V^{ijij}_{\mathbf{q}}}{D}, \tag{B8}$$

where $\{i,j\}=\{1,2\},\{2,1\}$ and

$$\mathcal{V}^2_{\mathbf{q}}=(V^{1212}_{\mathbf{q}})^2-V^{1111}_{\mathbf{q}}V^{2222}_{\mathbf{q}}, \tag{B9}$$

$$D=1-V^{1111}_{\mathbf{q}}\Pi^{11}-V^{2222}_{\mathbf{q}}\Pi^{22}-\mathcal{V}^2_{\mathbf{q}}\Pi^{11}\Pi^{22}.$$

In the static, long-wavelength limit[27] $\Pi^{ii}=-(\mathcal{A}m_i/\pi\hbar^2)f^i_{\mathbf{k}=0}$. For interactions which involve intersubband transitions, i.e., $V^{1221}_{\mathbf{q}}=V^{2112}_{\mathbf{q}}=V^{1122}_{\mathbf{q}}=V^{2211}_{\mathbf{q}}$, the form-factor $\mathcal{F}^{abcd}_{\mathbf{q}}$ tends to zero as $|\mathbf{q}|\to 0$, and cancels with the divergence in the unscreened Coulomb interaction in this limit. Because of this cancellation, these interactions are short range even in the absence of any screening. If they are screened similar to $V^{ijij}_{\mathbf{q}}$ this tends to overestimate the screening, resulting in a large underestimation of intersubband scattering rates.[28] Instead these matrix elements are replaced by[27]

$$\frac{V^{1221}_{\mathbf{q}}}{1-V^{1221}_{\mathbf{q}}(\Pi^{12}+\Pi^{21})} \tag{B10}$$

with $\Pi^{12}=(\mathcal{A}/\Delta E_{12})(N_1-N_2)$ where $\Delta E_{12}=\epsilon^1_{\mathbf{k}=0}-\epsilon^2_{\mathbf{k}=0}$ is the energy separation between subbands 1 and 2, and N_i is the carrier density in subband *i*.

APPENDIX C: DIPOLE DENSITY

The dipole density $\mathbf{P}^{(n)}(z',\omega)$ is determined by the sum of the IS coherences at all momenta $p^{(n)21}(\omega)=\Sigma_{\mathbf{k}}p^{(n)21}_{\mathbf{k}}(\omega)$. In the case of linear absorption, the Fourier transformation of $\Sigma_{\mathbf{k}}(d/dt)p^{21}_{\mathbf{k}}$ [see Eqs. (3) and (B3) –(B5)] yields an equation linear in $\int dz\mathbf{d}_{ab}(z)\cdot\mathbf{E}(z,\omega)$

$$p^{(n)21}(\omega)=\chi^{(n)}(\omega)\int dz\mathbf{d}^{(n)}_{ab}(z)\cdot\mathbf{E}^{(n)}(z,\omega), \tag{C1}$$

where the linear susceptibility $\chi^{(n)}$ is independent of the electric field

$$\chi^{(n)}(\omega)=\frac{p^{(n)21}(\omega)}{\frac{1}{\hbar}\int dz\mathbf{d}^{(n)}_{ab}(z)\cdot\mathbf{E}^{(n)}(z,\omega)} \tag{C2}$$

$$=\frac{\hat{p}^{21}(\omega)}{\frac{1}{\hbar}\mathbf{E}^{(n)}(z_0,\omega)\int dz\mathbf{d}^{(n)}_{ab}(z)}. \tag{C3}$$

In this notation $\hat{p}^{21}(\omega)$ denotes the IS coherence obtained by approximating $\int dz\mathbf{d}^{(n)}_{ab}(z)\cdot\mathbf{E}^{(n)}(z,\omega)\approx\mathbf{E}^{(n)}(z_0,\omega)\int dz\mathbf{d}^{(n)}_{ab}(z)$ in Eq. (B3b) where z_0 is the center of quantum well *n*. Using Eq. (C1) we can rewrite Eq. (1a) and obtain the dipole density $\mathbf{P}^{(n)}(z',\omega)$ as a function of the local field $\mathbf{E}^{(n)}(z,\omega)$ as given in Eq. (1b).

*Present address: Lawrence Berkeley National Laboratory, Berkeley, CA 94720.

[1] H. Haug and S.W. Koch, *Quantum Theory of the Optical and Electronic Properties of Semiconductors* (World Scientific, Singapore, 1994); H. Haug and A.-P. Jauho, *Quantum Kinetics in Transport and Optics of Semiconductors* (Springer, Berlin, 1996).

[2] M. Lindberg and S.W. Koch, Phys. Rev. B **38**, 3342 (1988); F. Rossi, S. Haas, and T. Kuhn, Phys. Rev. Lett. **72**, 152 (1994); F. Jahnke, M. Kira, S.W. Koch, G. Khitrova, E.K. Lindmark, T.R. Nelson, Jr., D.V. Wick, J.D. Berger, O. Lyngnes, H.M. Gibbs, K. Tai, *ibid.* **77**, 5257 (1996); S. Hughes, A. Knorr, S.W. Koch, R. Binder, R. Indik, and JV. Moloney, Solid State Commun. **100**, 555 (1996).

[3] T. Elsaesser and M. Woerner, Phys. Rep. **321**, 253 (1999).

[4] U. Ekenberg, Phys. Rev. B **40**, 7714 (1989).

[5] B.R. Nag and S. Mukhopadhyay, Phys. Status Solidi B **175**, 103 (1993).

[6] R.J. Warburton, C. Gauer, A. Wixforth, J.P. Kotthaus, B. Brar, and H. Kroemer, Phys. Rev. B **53**, 7903 (1996).

[7] D.E. Nikonov, A. Imamoğlu, L.V. Butov, and H. Schmidt, Phys. Rev. Lett. **79**, 4633 (1997).

[8] B. Nottelmann, V.M. Axt, and T. Kuhn, Physica B **272**, 234 (1999).

[9] S.V. Faleev and M.I. Stockman, Phys. Rev. B **66**, 085318 (2002).
[10] A. Liu, Phys. Rev. B **55**, 7796 (1997).
[11] M. Zaluzny and C. Nalewajko, Phys. Rev. B **59**, 13 043 (1999).
[12] G. Weber and A. Alcalde, Phys. Rev. B **56**, 9619 (1997).
[13] C.A. Ullrich and G. Vignale, Phys. Rev. Lett. **87**, 037402 (2001).
[14] In general, the linewidth is influenced both by intrinsic dephasing processes of the coherent IS polarization and by imperfections of the actual sample like alloy disorder, well width fluctuations, and interface roughness. Because of the high perfection of the growth techniques used, especially molecular-beam epitaxy, today's high-quality samples have only very small structural inhomogeneities with a negligible influence on the linewidth. Since the theoretical results are compared with experiments on such high-quality samples, we do not include scattering due to interface roughness and impurities here. For the sample used in the experiment (sample A), time-resolved four-wave mixing measurements [R.A. Kaindl, K. Reimann, M. Woerner, T. Elsaesser, R. Hey, and K. H. Ploog, Phys. Rev. B **63**, 161308 (2001)] have shown that inhomogeneous broadening has a negligible influence.
[15] F. Eickemeyer, M. Woerner, A.M. Weiner, T. Elsaesser, R. Hey, and K.H. Ploog, Appl. Phys. Lett. **79**, 165 (2001).
[16] J.E. Sipe, J. Opt. Soc. Am. B **4**, 481 (1987).
[17] T. Stroucken, A. Knorr, P. Thomas, and S.W. Koch, Phys. Rev. B **53**, 2026 (1996).
[18] T. Kuhn, in *Theory of Transport Properties of Semiconductor Nanostructures*, edited by E. Schöll (Chapman and Hall, London, 1998), p. 173.
[19] I. Waldmüller, M. Woerner, J. Förstner, and A. Knorr, Phys. Status Solidi B **238**, 474 (2003); I. Waldmüller, J. Förstner, and A. Knorr, in *Nonequilibrium Physics at Short Time Scales*, edited by K. Morawetz (Springer, Berlin, 2004).
[20] B. Robertson, Phys. Rev. **144**, 151 (1966); E. Fick and G. Sauermann, *The Quantum Statistics of Dynamical Processes* (Springer, Berlin, 1990).
[21] J. Förstner, K.J. Ahn, J. Danckwerts, M. Schaarschmidt, I. Waldmüller, C. Weber, and A. Knorr, Phys. Status Solidi B **234**, 155 (2002).
[22] W. Kohn, Phys. Rev. **123**, 1242 (1961); L. Brey, J. Dempsey, N.F. Johnson, and B.I. Halperin, Phys. Rev. B **42**, 1240 (1990); S.K. Yip, *ibid.* **43**, 1707 (1991).
[23] M. Braun and U. Rössler, J. Phys. C **18**, 3365 (1985).
[24] R.C. Iotti and F. Rossi, Phys. Rev. Lett. **87**, 146603 (2001).
[25] The random-phase approximation is based on the assumption that the kinetic energy is much greater than the Coulomb interaction energy between the electrons. This assumption is valid at high densities since the kinetic energy goes as $1/r_s^2$, while the potential energy goes as $1/r_s$, where r_s is a measure of the electron separation. [See G. Mahan, *Many-particle Physics*, 3rd ed. (Kluwer/Plenum, New York, 2000), p. 296.] For this reason, the RPA is often said to hold only at high densities. However, at high temperatures the kinetic energy increases, and the validity of the RPA extends to low densities. [H. Haug and S. Schmitt-Rink, Prog. Quantum Electron. **9**, 3 (1984), p. 35].
[26] J. Li and C.Z. Ning, Phys. Rev. Lett. **91**, 097401 (2003).
[27] S.-C. Lee and I. Galbraith, Phys. Rev. B **59**, 15 796 (1999).
[28] S.-C. Lee and I. Galbraith, Physica B **272**, 237 (1999).